Contact Angle Dependence on the Fluid−Wall Dispersive Energy

Martin Horsch,[†] Martina Heitzig,[‡,#] Calin Dan,[§] Jens Harting,[§,||] Hans Hasse,[⊥] and
Jadran Vrabec*,[†]

[†]*Thermodynamics and Energy Technology (ThEt), Universität Paderborn, Warburger Strasse 100,
33098 Paderborn, Germany,* [‡]*Institute of Thermodynamics and Thermal Process Engineering (ITT),
Universität Stuttgart, Pfaffenwaldring 9, 70569 Stuttgart, Germany,* [§]*Institute for Computational Physics
(ICP), Universität Stuttgart, Pfaffenwaldring 27, 70569 Stuttgart, Germany,* [||]*Department of Applied Physics
(TN), Technische Universiteit Eindhoven, P.O. Box 513, 5600 MB Eindhoven, The Netherlands, and*
[⊥]*Laboratory of Engineering Thermodynamics (LTD), University of Kaiserslautern, Erwin-Schrödinger-
Strasse 44, 67663 Kaiserslautern, Germany.* [#]*Current address: Computer Aided Process-Product Engineering
Center (CAPEC), Technical University of Denmark, Søltofts Plads, 2800 Kgs. Lyngby, Denmark*

Menisci of the truncated and shifted Lennard-Jones fluid between parallel planar walls are investigated by molecular dynamics simulation. Thereby, the characteristic energy of the unlike dispersive interaction between fluid molecules and wall atoms is systematically varied to determine its influence on the contact angle. The temperature is varied as well, covering most of the range between the triple-point temperature and the critical temperature of the bulk fluid. The transition between obtuse and acute angles is found to occur at a temperature-independent magnitude of the fluid−wall dispersive interaction energy. On the basis of the present simulation results, fluid−wall interaction potentials can be adjusted to contact angle measurements.

Introduction

A major challenge for molecular modeling consists of the definition of unlike interaction potentials. In the past, a variety of combination rules were proposed, none of which were found to be valid in general. Several of these, including the Lorentz−Berthelot combination rule, are considered to be a good starting point for further adjustment in most cases.[1] The present work contributes to our understanding of the dispersive interaction between a solid wall and a fluid, which is essential for the analysis of adsorption and microscopic flow properties.

In principle, the Lorentz−Berthelot rule can be applied for effective pair potentials acting between the fluid particles and the atoms of a solid wall[2,3] on the basis of size and energy parameters derived from properties of the solid and the fluid. Although using combination rules to extrapolate from homogeneous bulk solid and fluid properties to interfacial phenomena can lead to good agreement with the actual behavior,[2] this approach has only shaky theoretical foundations.[4] Unlike pair potentials between a fluid and a solid can be expected to give reliable results only if they are developed using actual information on fluid−wall contact effects. Because adsorption in nanopores can be studied on the basis of effective pair potentials,[3,5−8,9a,9b] it is conversely possible

to fit model parameters to adsorption isotherms.[10] The present study follows the line of research, suggested by Werder et al.,[11] of adjusting unlike parameters to contact angle measurements.

Using density functional theory, Teletzke et al.[12] examined the dependence of wetting and drying transitions on the characteristic size and energy parameters of the fluid−wall dispersive interaction. Subsequently, Sokołowski and Fischer[13] as well as Giovambattista et al.[14] investigated fluid density profiles in extremely narrow channels for several values of the fluid−wall dispersive energy and surface polarity, respectively. On the microscopic and nanoscopic levels, the statics and dynamics of fluids under confinement and the corresponding three-phase contact lines can also be investigated by the lattice Boltzmann method.[15−18]

Molecular dynamics (MD) simulation can be applied to this problem as well, leading to a consistent molecular approach. The increase in computing power and the development of massively parallel MD software provide tools for simulating systems with a large number of particles. System sizes accessible to MD simulation are getting closer to the smallest experimental settings. This allows us to compare simulation data directly to experimental observables for a growing spectrum of properties, including the

(1) Schnabel, T.; Vrabec, J.; Hasse, H. *J. Mol. Liq.* **2007**, *130*, 170–178.
(2) Steele, W. A. *J. Phys. Chem.* **1978**, *82*, 817–821.
(3) Schapotschnikow, P.; Pool, R.; Vlugt, T. J. H. *Comput. Phys. Commun.* **2007**, *177*, 154–157.
(4) Dzyaloshinskii, I. E.; Lifshitz, E. M.; Pitaevskii, L. P. *Adv. Phys.* **1961**, *10*, 165–209.
(5) Steele, W. A. *The Interaction of Gases with Solid Surfaces*; Pergamon: Oxford, U.K., 1974.
(6) Findenegg, G. H.; Fischer, J. *Faraday Discuss. Chem. Soc.* **1975**, *59*, 38–45.
(7) Fischer, J.; Bohn, M.; Körner, B.; Findenegg, G. H. *Chem. Ing. Tech.* **1982**, *54*, 763.
(8) Bucior, K.; Yelash, L.; Binder, K. *Phys. Rev. E* **2009**, *79*, 031604.
(9) (a) Schapotschnikow, P.; Hommersom, B.; Vlugt, T. J. H. *J. Phys. Chem. C* **2009**, *113*, 12690–12698. (b) Sokołowski, S.; Fischer, J. *Mol. Phys.* **1990**, *70*, 1097–1113.

(10) Vishnyakov, A.; Ravikovitch, P. I.; Neimark, A. V. *Langmuir* **1999**, *15*, 8736–8742.
(11) Werder, T.; Walter, J. H.; Jaffe, R. L.; Halicioglu, T.; Koumoutsakos, P. *J. Phys. Chem. B* **2003**, *107*, 1345–1352.
(12) Teletzke, G. F.; Scriven, L. E.; Davis, H. T. *J. Chem. Phys.* **1982**, *78*, 1431–1439.
(13) Sokołowski, S.; Fischer, J. *J. Chem. Soc., Faraday Trans.* **1993**, *89*, 789–794.
(14) Giovambattista, N.; Rossky, P. J.; Debenedetti, P. G. *Phys. Rev. E* **2006**, *73*, 041604.
(15) Harting, J.; Kunert, C.; Herrmann, H. J. *Europhys. Lett.* **2006**, *75*, 328–334.
(16) Diotallevi, F.; Biferale, L.; Chibbaro, S.; Puglisi, A.; Succi, S. *Phys. Rev. E* **2008**, *78*, 036305.
(17) Diotallevi, F.; Biferale, L.; Chibbaro, S.; Pontrelli, G.; Succi, S.; Toschi, F. *Eur. Phys. J. Spec. Top.* **2009**, *166*, 111.
(18) Spencer, T. J.; Hollis, A. P.; Halliday, I.; Care, C. M. *Proceedings of the 2nd Micro and Nano Flows Conference*; London, 2009, ISBN 978-1902316734.
(19) Allen, M. P.; Tildesley, D. J. *Computer Simulation of Liquids*; Clarendon Press: Oxford, U.K., 1987.

contact angle. The truncated and shifted Lennard-Jones (LJTS) potential[19] is used in the present work to describe both the fluid−fluid and the fluid−wall interactions, leading to systems that extend previous studies on interface properties for the LJTS fluid.[20−22] Hysteresis[23] as well as the formation and growth of liquid precursor layers on the surface[4] are not discussed because the present work deals with equilibrium properties of the phase boundary only.

Model and Simulation Method

Like the original Lennard-Jones (LJ) potential $u^{LJ}(r) = 4\varepsilon[(\sigma/r)^{12} - (\sigma/r)^6]$, the LJTS model[19]

$$u_{ij}^{ts}(r_{ij}) = \begin{cases} u^{LJ}(r_{ij}) - u^{LJ}(r_c) & r_{ij} < r_c \\ 0 & r_{ij} \geq r_c \end{cases} \quad (1)$$

with a cutoff radius of $r_c = 2.5\sigma$ accurately reproduces the thermophysical properties of several nonpolar fluids, in particular, noble gases and methane, when adequate values for size and energy parameters σ and ε, respectively, are specified.[20] Because of the relatively small cutoff radius, molecular simulation is comparably fast whereas the full descriptive power of the LJ potential is retained even for systems with phase boundaries.[20]

To describe the properties of a solid material accurately, it is usually necessary to employ multibody potentials that have a large number of model parameters and are computationally quite expensive.[24−26] The present study, however, does not regard the properties of a specific wall material but rather the influence of the fluid−wall dispersive interaction on the fluid itself. Accordingly, a layered wall was represented here by a comparably straightforward system of coupled harmonic oscillators using different spring constants D_y and D_{xz} for the transverse vibration with respect to the layers

$$u_i^y(y_i) = \frac{D_y}{2}(y_i - y_i^\circ)^2 \quad (2)$$

where y_i° is the equilibrium value of the y coordinate (i.e., the direction perpendicular to the wall), and longitudinal oscillations,
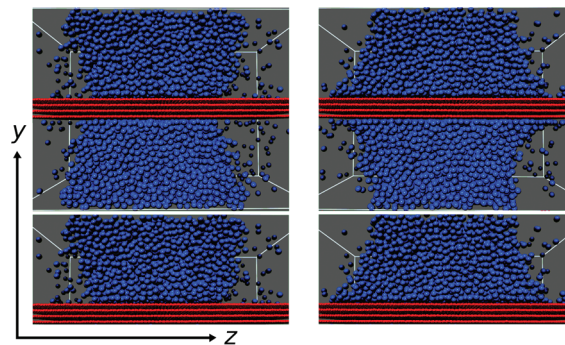
$$u_{ij}^{xz}(r_{ij}) = \frac{D_{xz}}{2}(r_{ij} - r_{ij}^\circ)^2 \quad (3)$$

are given with respect to the equilibrium bond length r_{ij}° between neighboring atoms i and j.

Fluid−wall interactions can be represented by full[5] or slightly modified[27] LJ potentials acting between fluid particles and the atoms of the solid. Following this approach, the LJTS potential with size and energy parameters $\sigma_{fw} = \sigma$ and

$$\varepsilon_{fw} = \zeta\varepsilon \quad (4)$$

was applied for the unlike interaction using the same cutoff radius as for the fluid. Potential parameters for the molecular models of

(20) Vrabec, J.; Kedia, G. K.; Fuchs, G.; Hasse, H. *Mol. Phys.* **2006**, *104*, 1509–1527.
(21) Horsch, M.; Vrabec, J.; Hasse, H. *Phys. Rev. E* **2008**, *78*, 011603.
(22) Horsch, M.; Vrabec, J.; Bernreuther, M.; Hasse, H. *Proceedings of the 6th International Symposium Turbulence, Heat and Mass Transfer*; **2009**, ISBN 978-1-56700-262-1.
(23) Monson, P. A. *Langmuir* **2008**, *24*, 12295–12302.
(24) Tersoff, J. *Phys. Rev. Lett.* **1988**, *61*, 2879–2882.
(25) Engin, C.; Sandoval, L.; Urbassek, H. M. *Modell. Simul. Mater. Sci. Eng.* **2008**, *16*, 035005.
(26) Ghiringhelli, L. M.; Valeriani, C.; Los, J. H.; Meijer, E. J.; Fasolino, A.; Frenkel, D. *Mol. Phys.* **2008**, *106*, 2011–2038.
(27) Dong, T.; Yang, Z.; Wu, H. *Energy Convers. Manage.* **2006**, *47*, 2178–2191.

Figure 1. Simulation snapshots for the reduced fluid−wall dispersive energy, $\zeta = 0.09$ (left) and 0.16 (right), at a temperature of $T = 0.73\varepsilon/k$. The upper half is reproduced in the bottom to illustrate the effect of the periodic boundary condition.

the fluid as well as the solid component were chosen to represent methane and graphite, respectively. For the fluid, LJTS size and energy parameters $\sigma = 3.7241$ Å and $\varepsilon/k = 175.06$ K as well as molecular mass $m = 16.04$ u were used[20] so that the carbon−carbon (C−C) bond length in graphite, $r_{ij}^\circ = 1.421$ Å,[28] can be expressed in LJ units as $r_{ij}^\circ = 0.3816\sigma$ and the interlayer distance $Y = 3.35$ Å corresponds to 0.8996σ.

The spring constant $D_{xz} = 15600$ N/m related to the sp² bonds was adjusted to the C−C radial distribution function obtained from simulations with the Tersoff[24] potential for a system consisting of seven graphite layers with 7052 carbon atoms per layer. This distribution had to be rescaled because, as previously shown,[22,29] the Tersoff potential deviates by about 3% from the actual bond length in graphite. In agreement with the relation between the C−C bond energy (4.3 eV) and the interaction energy between adjacent graphite layers (0.07 eV),[30] the interlayer spring constant was specified as $D_y = D_{xz}/60$. Equations 2 and 3 ensure that the wall atoms oscillate around the fixed y coordinate that corresponds to their layer whereas no particular x and z coordinates are preferred because the atoms are connected only to their immediate neighbors to permit individual sliding of the wall layers.

Parallel canonical ensemble MD simulations were conducted with the program *ls1 mardyn*[31] using spatial domain decomposition based on a linked cell data structure to obtain the contact angle dependence on the temperature and the reduced fluid−wall dispersive energy. For all simulation runs, Newton's equations of motion were integrated according to the Verlet leapfrog algorithm with a time step of 1 fs (i.e., $8.09 \times 10^{-4} \varepsilon^{-1/2} m^{1/2} \sigma$ in LJ units). Vapor and liquid were independently equilibrated in homogeneous simulations for 10 ps. This was followed by 200 ps of equilibration for the combined system (i.e., a liquid slab surrounded by vapor, overall containing between 13 600 and 15 800 fluid particles), with a wall consisting of 4 layers containing 7052 carbon atoms per layer (cf. Figure 1), where the starting configuration contained a planar vapor−liquid interface perpendicular to the z coordinate axis. The length of the simulation box for the combined system was 29.1σ in the x direction, 32.0σ in the y direction, and 46.1σ in the z direction in all cases. Note that the distance from the wall is given by the y coordinate and z is the characteristic direction for the density gradient of the fluid.

(28) Wiberg, N. *Holleman-Wiberg Inorganic Chemistry*; Academic Press: San Diego, CA, 2001.
(29) Kelires, P. C. *Phys. Rev. B* **1993**, *47*, 1829–1839.
(30) Cotton, F. A.; Wilkinson, G.; Gaus, P. L. *Basic Inorganic Chemistry*; Wiley: Chichester, U.K., 1994.
(31) Bernreuther, M.; Niethammer, C.; Horsch, M.; Vrabec, J.; Deublein, S.; Hasse, H.; Buchholz, M. *Innovatives Supercomputing Deutschland* **2009**, *7*, 50–53.
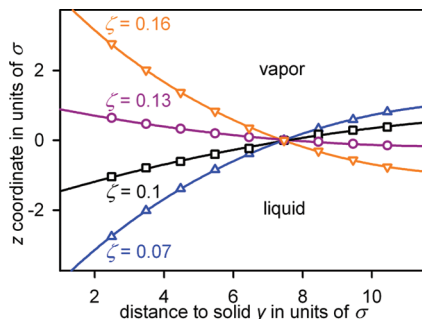
Figure 2. Vapor−liquid interface profiles for the reduced fluid−wall dispersive energy of $\zeta = 0.07$ (△), 0.10 (□), 0.13 (○), and 0.16 (▽) at a temperature of $T = 0.82\varepsilon/k$. Note that the full lines are circle segments, adjusted to the data points that are represented by symbols. The almost perfect match between the individual simulation results, indicated by their collective agreement with the fit, reflects the precision of the present simulation data. At $T = 1\varepsilon/k$, however, the margin of error becomes more significant.

The periodic boundary condition was applied to the system, leaving a channel for the fluid with a height of 27.4σ between the wall and its periodic image.

Via binning, the density profiles were averaged over at least 800 ps after equilibration. The arithmetic mean density $\rho_{vl} = (\rho' + \rho'')/2$ was applied to define the position of the phase boundary, where ρ' and ρ'' are the saturated bulk densities of liquid and vapor that are known for the LJTS fluid from previous work.[20] In the immediate vicinity of the wall, the fluid is affected by short-range ordering effects.[8,15,32] The influence of this phenomenon was minimized by taking density averages over a bin size of about 1σ (cf. Figure 2) following Giovambattista et al.[33] A circle was adjusted to the positions of the interface in the bins corresponding to distances between 3σ and 11σ from the wall, and the tangent to this circle at a distance of 1σ from the wall was consistently used to determine the contact angle.

Simulation Results

Menisci between parallel planar walls were simulated for a reduced fluid−wall dispersive energy ζ between 0.07 and 0.16 at temperatures of 0.73, 0.82, 0.88, and 1 ε/k. Note that for the bulk LJTS fluid the triple-point temperature is about 0.65 ε/k according to van Meel et al.[34] and the critical temperature is 1.0779 ε/k according to Vrabec et al.[20] so that almost the entire regime of vapor−liquid coexistence was covered here.

High values of ζ correspond to a strong attraction between fluid particles and wall atoms, leading to a contact angle of $\vartheta < 90°$ (i.e., partial or perfect wetting of the surface). As expected, with increasing fluid−wall dispersive energy, the extent of wetting grows (cf. Figure 1). As can be seen in Table 1 and Figure 2, the transition from obtuse to acute contact angles occurs at ζ values between 0.11 and 0.13 over the whole studied temperature range. Present simulation results were correlated by

$$\cos \vartheta(T, \zeta) = \left(1 + \frac{\tau^{1.7}}{27}\right) \tanh \frac{\zeta - Z}{0.087} \qquad (5)$$

Table 1. Contact Angle of the LJTS Fluid on Graphite from MD Simulation as a Function of the Reduced Fluid−Wall Dispersive Energy and Temperature

	contact angle			
ζ	$kT/\varepsilon = 0.73$	$kT/\varepsilon = 0.82$	$kT/\varepsilon = 0.88$	$kT/\varepsilon = 1$
0.07	127°	134°	139°	180°
0.09	112°	116°	119°	180°
0.10	107°	106°	109°	145°
0.11	99°	95°	96°	128°
0.12			86°	86°
0.13	82°	79°	76°	81°
0.14	73°	67°	63°	0°
0.16	58°	45°	40°	0°
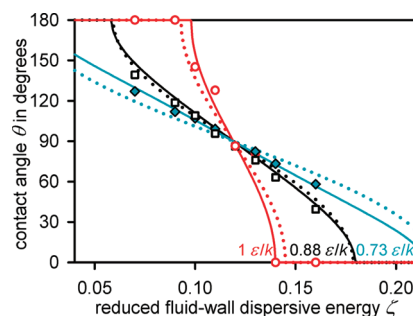
Figure 3. Simulation results for the contact angle as a function of the reduced fluid−wall dispersive energy ζ at temperatures of $T = 0.73\varepsilon/k$ (◇), $0.88\varepsilon/k$ (□), and $1\varepsilon/k$ (○) in comparison with the proposed correlation (−) (cf. eq 5) and the linear approximation (···) (cf. eqs 8 and 9), with $c = -7\sigma\varepsilon$.

where $\tau = (1 - (T/T_c))^{-1}$ approaches infinity for $T \rightarrow T_c$ and $Z = 0.119$ is the reduced fluid−wall dispersive energy that leads to a contact angle of $\vartheta = 90°$.

Perfect wetting or drying is present where eq 5 yields $\cos \vartheta \geq 1$ or $\cos \vartheta \leq -1$, respectively. In particular, both the value of Z and the symmetry relation

$$\cos \vartheta(T, Z - \Delta\zeta) = -\cos \vartheta(T, Z + \Delta\zeta) \qquad (6)$$

were found to be temperature-independent. Note that the simulation results strongly suggest such a symmetry property (cf. Figure 3), which is not an artifact of the correlation.

Figure 3 shows, particularly for high temperatures, that there is a narrow range of ζ values that lead to the formation of a contact angle as opposed to perfect wetting or drying. The present plots agree qualitatively with those determined by Giovambattista et al.[33] for the influence of the polarity of hydroxylated silica surfaces on the contact angle formed with water. In Figure 4, it can be seen that the extent of wetting (for $\zeta > Z$) or drying (for $\zeta < Z$), respectively, increases as the temperature approaches T_c. Eventually, this leads to the known phenomenon of critical point wetting[35] for the whole range above a wetting temperature T_w.

The effects described above can be accounted for by the Young equation

$$\cos \vartheta(T, \zeta) = \frac{\gamma_s(T, \zeta, \rho'') - \gamma_s(T, \zeta, \rho')}{\gamma(T)} \qquad (7)$$

which relates the vapor−liquid surface tension γ and the contact angle to the interfacial tension γ_s that acts between the wall and vapor or liquid. Qualitatively, the essential phenomena are
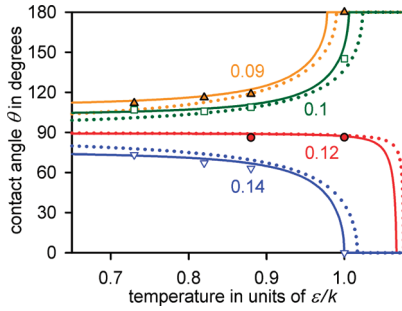
(32) Kozak, E.; Sokołowski, S. *J. Chem. Soc., Faraday Trans.* **1991**, *87*, 3415–3422.

(33) Giovambattista, N.; Debenedetti, P. G.; Rossky, P. J. *J. Phys. Chem. B* **2007**, *111*, 9581–9587.

(34) van Meel, J. A.; Page, A. J.; Sear, R. P.; Frenkel, D. *J. Chem. Phys.* **2008**, *129*, 204505.

(35) Cahn, J. W. *J. Chem. Phys.* **1977**, *66*, 3662–3672.

Figure 4. Simulation results for the contact angle as a function of the temperature at fluid−wall dispersive energies of $\zeta = 0.09$ ($\triangle$), 0.10 ($\square$), 0.12 ($\bigcirc$), and 0.14 ($\triangledown$) in comparison to the proposed correlation (−) (cf. eq 5) and the linear approximation (···) (cf. eqs 8 and 9) with $c = -7\sigma\varepsilon$. The entire temperature range between the triple point and the critical point of the bulk fluid is shown.

reproduced by assuming a linear dependence of the fluid−wall surface tension on the fluid density as well as the magnitude of the fluid−wall interaction

$$\left(\frac{\partial^2 \gamma_s}{\partial \zeta \partial \rho}\right)_T = c \tag{8}$$

with

$$\left(\frac{\partial \gamma_s}{\partial \rho}\right)_{\zeta,\, T}\bigg|_{\zeta = Z} = 0 \tag{9}$$

wherein ρ refers to the density of the fluid. For $c \approx -7\sigma\varepsilon$, good quantitative agreement is obtained (cf. Figures 3 and 4) using the values of Vrabec et al.[20] for the density of the bulk fluid phases and the vapor−liquid surface tension. This illustrates that despite its nanoscopic dimension, the Young equation and related concepts, such as effective dividing surfaces between the fluid phases as introduced by Gibbs, are fully applicable to the investigated system geometry.

The deviation of the contact angle from 90° increases with $T \rightarrow T_c$ because $\gamma(T)$ converges to zero faster than does the density difference $\rho'(T) - \rho''(T)$ between the two fluid phases. The relevant critical exponents in the case of the LJTS fluid are

$$\lim_{T \rightarrow T_c} \frac{\ln[\rho'(T) - \rho''(T)]}{\ln(T_c - T)} \approx \frac{1}{3} \tag{10}$$

for the saturated densities of the bulk fluid,[20] in accordance with the Guggenheim[36] approach, and

$$\frac{d \ln \gamma(T)}{d \ln(T_c - T)} \approx 1.21 \tag{11}$$

for the vapor−liquid surface tension,[20] confirming a similar value (1.26) obtained from the fluctuation theory of critical phenomena.[37]

The correlation given by eq 5 suggests for the present system a first-order transition between partial and perfect wetting or drying, respectively, as described by Cahn.[35] With $\zeta \approx Z$, Figure 3 shows that the contact angle ϑ depends linearly on the fluid−wall

(36) Guggenheim, E. A. *J. Chem. Phys.* **1945**, *13*, 253–261.
(37) Anisimov, M. A. *Critical Phenomena in Liquids and Liquid Crystals*; Nauka: Moscow, 1987.

dispersive energy and the symmetry property suggests for $\zeta = Z$ that γ_s does not depend on the density of the fluid.

Comparative Discussion

Qualitatively, the symmetry relation given by eq 6 corroborates the results of Monson,[23] who obtained the same property based on mean-field DFT calculations. If each layer of the wall is approximated as a plane of uniform density η, then the well depth of the fluid−wall dispersive interaction, which can be used to compare different interaction models quantitatively, is given by

$$W = -\eta\zeta \min_{y>0} \int_0^\infty d\lambda\, 2\pi\lambda \sum_{\ell=0}^{L-1} u^{ts}([(y + \ell Y)^2 + \lambda^2]^{1/2}) \tag{12}$$

for a system of L layers with an interlayer distance of Y. In the present case with $r_c = 2.5\sigma$ for the LJTS potential as well as a surface density of $\eta = 5.287\sigma^{-2}$, an interlayer distance of $Y = 0.8996\sigma$, and the number of layers $L = 3$ (the fourth layer of the wall is beyond the cutoff radius), one obtains

$$W = 17.29 kT_c \zeta \tag{13}$$

normalized by the critical temperature $T_c = 1.0779\varepsilon/k$ of the bulk LJTS fluid.[20] The transition from obtuse to acute contact angles, occurring at $Z = 0.119$ in the present case, therefore corresponds to a well depth of $W_z = 2.057 kT_c$.

A very similar system was investigated by Bucior et al.,[8] albeit for the LJTS fluid with a cutoff radius of $2^{7/6}\sigma$ as well as a rigid wall with a surface density of $\eta = 1.7342\sigma^{-2}$ and a single solid layer (i.e., $L = 1$). For that fluid, the critical temperature is given by Schrader et al.[38] as $T_c = 0.9999\varepsilon/k$ so that the fluid−wall dispersive energy was related to the well depth by $W = 5.429 kT_c \zeta$ according to eq 12. From the density profiles of Bucior et al.,[8] one finds that a rectangular contact angle is reached for a reduced fluid−wall dispersive energy of ζ between 0.61 and 0.7 (i.e. $3.3 kT_c < W_z < 3.8 kT_c$), which is of the same order of magnitude as the present result. The quantitative deviation has to be attributed to the different solid structure because the single wall layer of Bucior et al.[8] leads to a faster decay of the fluid−wall dispersion with respect to the distance than in the present simulations where three layers can directly interact with the fluid. A larger value of $W_z/(kT_c)$ is required to compensate for the effectively smaller length scale of the dispersive interaction.

The present correlation (cf. eq 5) predicts perfect wetting for

$$T_w\left(\frac{W}{kT_c}\right)$$

$$= \left(1 - 0.144\left[\left(\tanh\left[0.665\frac{W}{kT_c} - 1.37\right]\right)^{-1} - 1\right]^{-0.588}\right) T_c \tag{14}$$

The transition to perfect wetting was also simulated by Bojan et al.,[39] who applied the Monte Carlo method in the grand canonical ensemble to neon on metal surfaces. Thereby, the full LJ fluid, with $T_c = 1.310\varepsilon/k$ as determined by Lotfi et al.,[40] was used to model neon. With $W = 2.13 kT_c$, representing magnesium,

(38) Schrader, M.; Virnau, P.; Binder, K. *Phys. Rev. E* **2009**, *79*, 061104.
(39) Bojan, M. J.; Stan, G.; Curtarolo, S.; Steele, W. A.; Cole, M. W. *Phys. Rev. E* **1999**, *59*, 864–873.
(40) Lotfi, A.; Vrabec, J.; Fischer, J. *Mol. Phys.* **1992**, *76*, 1319–1333.

they obtained a wetting temperature of $T_w \approx 0.50 T_c$ as opposed to the present results that imply that perfect wetting is reached only above $0.974 T_c$, in the immediate vicinity of the critical temperature.

As Bojan et al.[39] themselves remark, their calculations predict a much lower wetting temperature than does a similar previous study by Sokołowski and Fischer[41] on the local structure of fluid argon in contact with solid carbon dioxide (with the same value of W/ε). The latter MD simulation results used a size parameter σ_{fw}/σ that is significantly smaller than unity in the case of argon and carbon dioxide[32,41] and therefore cannot be directly compared to the present work because varying the interaction length scale can lead to qualitatively different properties such as a change in the order of the wetting transition.[12] However, it should be pointed out that significantly better agreement was obtained here with the results of Sokołowski and Fischer[41] than with those of Bojan et al.[39]

The results presented above can now be used to provide an estimate of the magnitude of the dispersive interaction between fluids and wall materials for which experimental data on the contact angle are available. For instance, regarding the refrigerant R134a (1,1,1,2-tetrafluoroethane) at temperatures between 10 and 80 °C, Vadgama and Harris[42] obtained contact angles of $5.5 \pm 1°$ on copper and $7 \pm 1°$ on aluminum. With $T = 0.85 T_c$, which is 45 °C for R134a, the well depth can be estimated to be $W/k \approx 2.9 T_c = 1100$ K in both cases on the basis of eqs 5 and 13.

This can be related to a molecular model of the dispersive interaction by

$$W = -\rho_w \min_{y>0} \int_0^\infty d\lambda \, 2\pi\lambda \int_0^\infty dv \, u_{fw}([(y+v)^2 + \lambda^2]^{1/2}) \tag{15}$$

wherein ρ_w is the density of the solid wall and u_{fw} is the dispersive interaction potential acting between a fluid molecule and a wall atom. Note that whereas eq 12 corresponds to a sum over truncated and shifted LJ-10-4 terms, eq 15 does not rely on any particular assumption on the internal structure of the solid wall. If, for example, an LJ-12-6 potential is used for u_{fw}, then it corresponds to an LJ-9-3 interaction. This reasoning can plausibly be applied to all fluids that do not exhibit an excessively polar or anisotropic structure.

(41) Sokołowski, S.; Fischer, J. *Phys. Rev. A* **1990**, *41*, 6866–6870.
(42) Vadgama, B.; Harris, D. K. *Exp. Therm. Fluid Sci.* **2007**, *31*, 979–984.

Conclusions

The contact angle formed between a wall and a vapor−liquid interface was determined by canonical ensemble MD simulation for nonpolar fluids with equal length scales for the fluid−fluid and fluid−wall dispersive interactions whereas the magnitude of the fluid−wall dispersive interaction and the temperature were varied. Over the whole temperature range under investigation, the contact angle dependence on the fluid−wall dispersive energy was found to follow a simple symmetry law, whereby the dependence on the temperature is qualitatively covered by the Young equation, leading to a first-order transition to perfect wetting or drying at high temperatures. At a temperature-independent value of the reduced fluid−wall dispersive energy, the interfacial tensions between vapor and solid as well as liquid and solid are equal, corresponding to the transition between obtuse and acute contact angles.

The present MD simulation results can be expected to carry over to macroscopic systems because a qualitative influence of the wall on the vapor−liquid interface profile, as determined by an arithmetic mean density criterion, was detected only in the immediate vicinity of the wall. At temperatures of $0.88 \varepsilon/k$ and below, in particular, the phase boundary was found to be almost perfectly cylindrical for a distance from the wall exceeding 2.5σ, which approximately corresponds to a nanometer. The generality of the present findings is, however, limited to systems where the interaction between fluid molecules and the fluid−wall interaction are dominated by dispersion as opposed to electrostatics such that the characteristic length scales of the fluid−fluid and fluid−wall dispersion are similar. Furthermore, the effects of surface roughness were not discussed here, although they are clearly decisive for many practical applications.